Hybrid ZnO/Phthalocyanine Photovoltaic Device with Highly Resistive ZnO Intermediate Layer

Masanobu Izaki,*,[†,‡] Ryo Chizaki,[†] Takamasa Saito,[†] Kazufumi Murata,[†] Junji Sasano,[†] and Tsutomu Shinagawa[§]

[†]Graduate School of Engineering, Toyohashi University of Technology, Toyohashi, Aichi 441-8580, Japan
[‡]CREST, Japan Science and Technology Agency (JST), 5, Sanban-cho, Chiyoda-ku, Tokyo 102-0075, Japan
[§]Electronics Materials Department, Osaka Municipal Technical Research Institute, Osaka 536-8553, Japan

Ⓢ Supporting Information

ABSTRACT: We report a hybrid photovoltaic device composed of a 3.3 eV bandgap zinc oxide (ZnO) semiconductor and metal-free phthalocyanine layers and the effects of the insertion of the highly resistive ZnO buffer layer on the electrical characteristics of the rectification feature and photovoltaic performance. The hybrid photovoltaic devices have been constructed by electrodeposition of the 300 nm thick ZnO layer in a simple zinc nitrate aqueous solution followed by vacuum evaporation of 50−400 nm thick-phthalocyanine layers. The ZnO layers with the resistivity of 1.8×10^3 and 1×10^8 Ω cm were prepared by adjusting the cathodic current density and were installed into the hybrid photovoltaic devices as the n-type and buffer layer, respectively. The phthalocyanine layers with the characteristic monoclinic lattice showed a characteristic optical absorption feature regardless of the thickness, but the preferred orientation changed depending on the thickness. The ZnO buffer-free hybrid 50 nm thick phthalocyanine/n-ZnO photovoltaic device showed a rectification feature but possessed a poor photovoltaic performance with a conversion efficiency of 7.5×10^{-7} %, open circuit voltage of 0.041 V, and short circuit current density of 8.0×10^{-5} mA cm^{-2}. The insertion of the ZnO buffer layer between the n-ZnO and phthalocyanine layers induced improvements in both the rectification feature and photovoltaic performance. The excellent rectification feature with a rectification ratio of 3188 and ideally factor of 1.29 was obtained for the hybrid 200 nm thick phthalocyanine/ZnO buffer/n-ZnO photovoltaic device, and the hybrid photovoltaic device possessed an improved photovoltaic performance with the conversion efficiency of 0.0016%, open circuit voltage of 0.31 V, and short circuit current density of 0.015 mA cm^{-2}.

KEYWORDS: zinc oxide, phthalocyanine, hybrid, photovoltaic device, rectification
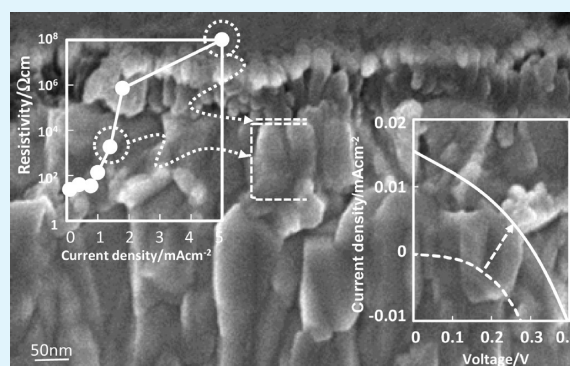
1. INTRODUCTION

Hybrid diodes composed of inorganic and organic semiconductors have attracted increasing attention in electronics applications, especially the photovoltaic device.[1] There have been many reports on hybrid ZnO diodes with organic semiconductors of polymers such as poly [2-methoxy-5-(3′,7′-dimethylocthyloxy)-1,4-phelene-vinylene] (MDMO-PPV)[2] and poly[3-hexylthiophene-2,5-diyl] (P3HT)[3] and with small molecules of phthalocyanine compounds.[4] The hybrid photovoltaic device with polymer semiconductors have been extensively studied by Mcghee[5] and Janssen groups, and a conversion efficiency up to 1.6% was reported for the ZnO/polymer hybrid photovoltaic device.[6] Also, the effects of the insertion of a polymer semiconductor and dyes between the inorganic and polymer semiconductor layers were investigated for modifying the heterointerface state.[7] In contrast, the conversion efficiency was limited at a very low level for the hybrid ZnO photovoltaic devices with small molecules, such as

hybrid ZnO photovoltaic devices with Ni[4] and Zn-phthalocyanine compounds.[8]

The phthalocyanine compounds are indispensable components as the donor for the high efficiency bulk-heterojunction organic photovoltaic device,[9] but the conversion efficiency was limited to a low level for the layered organic photovoltaic device with phthalocyanine compounds.[10] The mechanism for generating a photocurrent in a hybrid photovoltaic device is believed to be due to the creation of bound excitons by absorbing light in the active organic semiconductor of the devices.[11] The generation of carriers was resulted from the dissociation of excitons by the internal electric field generated at the interface of the inorganic semiconductor layer. The ZnO layer introduced into the hybrid photovoltaic device plays a role
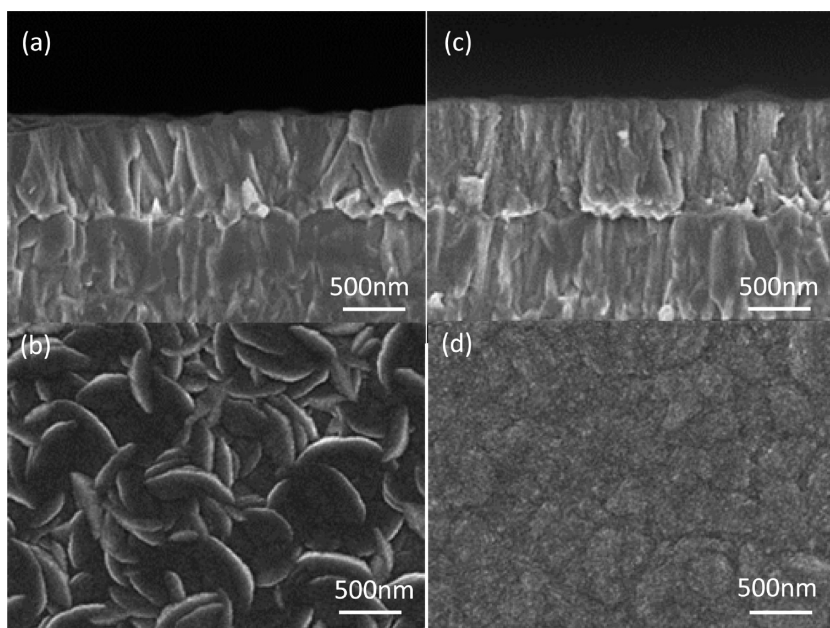
Figure 1. Cross-sectional and surface images for ZnO layers deposited at cathodic current density of (a, b) −1.4 and (c, d) −5.0 mA cm^{-2}.

in accelerating the dissociation of the excitons and reducing the recombination loss, and the ZnO layer does not act as a light-absorbing layer due to the band gap energy of 3.3 eV.

We have reported the construction of the layered hybrid Cu_2O/C_{60} photovoltaic device,[12] and the short circuit current density was extremely low compared to those for the Cu_2O/ZnO[13] and C_{60}/phthalocyanine photovoltaic device,[14] indicating that the photocurrent generated in both the Cu_2O and C_{60} layers could not be taken out for the hybrid structure. The importance of the Cu_2O/C_{60} heterointerface including the band alignment has been pointed out. It was generally agreed for a $Cu(InGa)Se_2$/n-ZnO solar cell that the band alignment including the conduction band offset strongly affected the conversion efficiency and was controlled by inserting buffer layers, such as CdS and Zn(O,S) layers, with the optimum electron state.[15]

The ZnO layer has been prepared by several techniques, such as the gas-phase deposition techniques of molecular beam epitaxy and sputtering, and by solution chemical processes, such as electrodeposition[16] and chemical deposition.[17] The solution chemical processes have several advantages over gas-phase deposition techniques and were recently used for the fabrication of the Cu_2ZnSnS_4 (CZTS)[18] and CIGS precursors[19] during solar cell production. The electrical characteristics of the electrodeposited ZnO semiconductor can be controlled over a wide range by adjusting the preparation conditions, such as the current density and solution temperature.[20] The electrodeposition technique allows the continuous deposition of ZnO layers with different electrical characteristics, which act as the n-type and highly resistive buffer layers, by controlling the preparation condition during the ZnO electrodeposition.

Here, we report the construction of the layered hybrid ZnO/phthalocyanine photovoltaic devices on a transparent conductive glass by electrodeposition of the ZnO layer followed by vacuum evaporation of the metal-free phthalocyanine layer, and the effects of the insertion of a highly resistive ZnO buffer layer between the n-ZnO and phthalocyanine layers on the electrical characteristics of the rectification feature and photovoltaic performance have been investigated. The n-type and highly

resistive ZnO buffer layers were prepared by controlling the cathodic current density and electric charge during the ZnO electrodeposition in a simple zinc nitrate aqueous solution, and the electrical and optical characterizations were performed. The hybrid phthalocyanine/n-ZnO photovoltaic device without the highly resistive ZnO buffer layer showed a poor photovoltaic performance, but the insertion of the highly resistive ZnO buffer layer induced improvements in both the rectification feature in dark and photovoltaic performance.

2. EXPERIMENTAL SECTION

The ZnO layer was prepared on a F-doped SnO_2-coated glass substrate (FTO, AGC Fabritech Co., Ltd.Type DU) by electrodeposition in an aqueous solution containing 0.08 mol/L zinc nitrate hydrate at 333K using a potentiostat (Hokuto Denko, HA-501) connected to a function generator (Hokuto Denko, HB-105) and coulomb meter (Hokuto Denko, HF-201). The solution was prepared with a reagent grade chemical and distilled water purified by a Millipore Elix Advantage. The 300-nm-thick n-ZnO layer was galvanostatically prepared at the cathodic current density of −1.4 mA cm^{-2} for 0.5 coulomb/cm^2, and then a ZnO buffer layer was stacked on the n-ZnO layer at −5.0 mA cm^{-2} for 0.05 C cm^{-2} by automatically controlling the current density using the function generator. The current densities were determined by preliminary experiments. The 750 nm thick ZnO layers for electrical and optical characterizations were prepared on the FTO substrate at −1.4 and −5.0 mA cm^{-2} for 1.25 C cm^{-2}.

The phthalocyanine layer was prepared by the vacuum evaporation of the phthalocyanine powder (Aldrich, 99.9% purity) using a vacuum evaporation system (ULVAC, VTS-350ERH/M) connected to a vacuum system consisting of a turbo molecular pump and oil-free scroll vacuum pump. The evaporation was carried out at ambient temperature and a vacuum of around 1.5×10^{-4} Pa, and the evaporation rate was controlled at 0.05 nm/s using a quartz crystal deposition control system (ULVAC, CRTM-6000G). The phthalocyanine/ZnO photovoltaic device was fabricated by stacking an Au electrode using the evaporation system.

The thickness was determined by a surface profile measurement system (ULVAC, DekTak150). The X-ray diffraction patterns were recorded by a $\theta/2\theta$ scanning technique with monochromated CuKα radiation operated at 40KV and 200 mA using a Rigaku RINT2500. The optical absorption spectra were recorded using a UV−vis−NIR
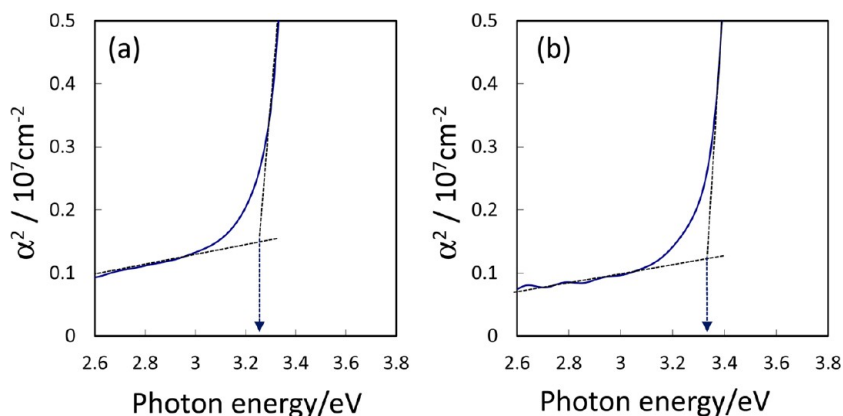
Figure 2. Correlation of absorption coefficient to photon energy for the ZnO layers deposited at cathodic current density of (a) −1.4 and (b) −5.0 mA cm^{-2}.
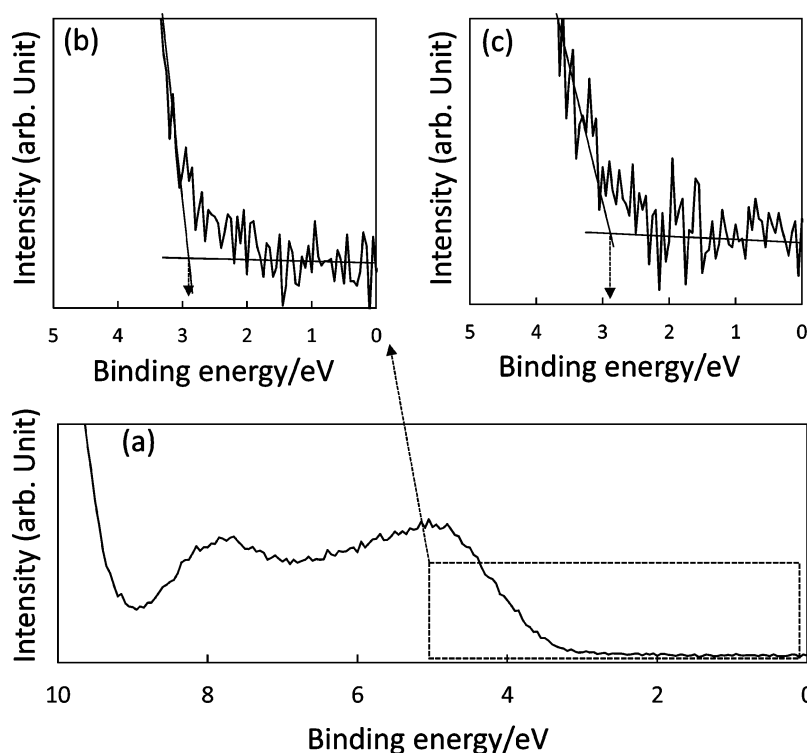
Figure 3. Valence band spectra for ZnO layers deposited at cathodic current density of (a, b) −1.4 and (c) −5.0 mAcm^{-2}.

spectrophotometer (Hitachi, U4100) with a reference to the bare substrate. Electron microscopic observations were carried out using a field-emission scanning electron microscope (FE-SEM, JEOL, JSM-6700F) and a field-emission transmission electron microscopy (FE-TEM, JEOL, JEM-2100F) at the accelerating voltage of 200 kV. The sample for the FE-TEM observation was prepared by mechanically cutting using a focused ion beam (FIB, FEI Quanta 3D) with a Ga ion beam after the coating the Pt layer over the sample surface by a vacuum evaporation in FIB. An X-ray photoelectron spectroscopy (XPS) analysis and valence band spectra measurements were performed using an ULVAC-PHI model 5700MC with monochro-meted Al Kα radiation at pressure of around 1.6×10^{-8} Pa. Binding energy was corrected by referencing the C1s signal of adventitious contamination hydrocarbon to 284.8 eV. The electron-pass energy in the analyzer was set at 11.75 eV, corresponding to 0.56 eV of full-width at half-maximum of the Ag 3d5/2 peak at 368.36 eV.

The electrical characteristic of both the ZnO and phthalocyanine layers were carried out by the van-der-Pauw method using a Hall effect measuring system (Toyo Technica, Resitest 8310) in air at ambient temperature and 0.3 T magnetic field. The ZnO sample was prepared by mechanically splitting them off from the glass substrate followed by fastening in epoxy resin (Araldite 2091). The phthalocyanine sample was prepared on a quartz glass substrate by evaporating the phthalocyanine in the same manner as that for constructing the hybrid photovoltaic device. Four In and Au electrodes were prepared on the ZnO and phthalocyanine samples, respectively, using a vacuum evaporation system (ULVAC, VPC-260F). The electrical characteristic was estimated by recording the current density−voltage curves using a solar simulator system with a Keithley 2400 source meter (Bunko Keiki, OTENTO-SUN III) in dark and under AM1.5G illumination with a 100 mW cm^{-2} power.

3. RESULTS AND DISCUSSION

3.1. Effects of Cathodic Current Density on the Electrical and Optical Characteristics of ZnO Layers.
Figure 1 shows FE-SEM images of the surface and cross-sectioned structures for the 750 nm thick ZnO layers prepared

at the cathodic current density of −1.4 and −5.0 mA cm^{-2}. The ZnO layer prepared at −1.4 mA cm^{-2} showed the (0002) preferred orientation based on an X-ray diffraction measurement. The ZnO layer was composed of aggregates of columnar grains grown in a direction normal to the surface, and the defects, such as pores, could not be located both on the surface and the cross-sectioned images. The ZnO layer prepared at −5.0 mA cm^{-2} showed a random orientation based on an X-ray diffraction measurement. The cross-sectioned structure was similar to that at −1.4 mA cm^{-2}, but the irregularity of approximately 30 nm in size could be observed on the side surface of the columnar ZnO grains. The surface morphology was different to that at −1.4 mA cm^{-2} and was composed of aggregates of granular grains with the size of 30 nm corresponding to that estimated from the cross-sectioned image.

The ZnO layer prepared at −1.4 mA cm^{-2} showed a resistivity of 1.8×10^3 Ω cm with a 1.6×10^{15} cm^{-3} in carrier concentration and 2.2 cm^2 V^{-1} s^{-1} in mobility. The ZnO layer prepared at −5.0 mAcm^{-2} showed a resistivity of 1×10^8 Ω cm, which was higher by 5 orders of magnitude than that at −1.4 mAcm^{-2}, but the carrier concentration and mobility could not be estimated by the van der Pauw method due to the high resistivity. However, it was speculated that the carrier concentration for the ZnO layer prepared at −5.0 mA cm^{-2} was lower than that at −1.4 mA cm^{-2}. (The dependence of the resistivity, carrier concentration, and mobility for the ZnO layers on the cathodic current density is not shown here; see the Supporting Information.)

Figure 2 shows the correlation between the absorption coefficient and photon energy for the ZnO layers prepared at −1.4 and −5.0 mA cm^{-2}. The absorption coefficient was calculated from the absorbance estimated from the absorption spectra and thickness estimated from the cross-sectioned images. The optical bandgap energy (E_g) was evaluated using the following dependence of the absorption coefficient (α) on the photon energy (E_{pt}),

$$\alpha^2 \propto (E_{pt} - E_g)$$

for the direct transition semiconductor. The bandgap energy was estimated to be 3.25 and 3.32 eV for the ZnO layers prepared at −1.4 and −5.0 mAcm^{-2}, respectively.

Figure 3 shows the valence band spectra recorded for the ZnO layers prepared at −1.4 and −5.0 mAcm^{-2}. The electron spectra were recorded after Ar sputtering for 10 min in order to remove the carbon and other surface contaminations, and it was confirmed that the states of Zn^{2+} and O^{2-} agreed with those in the ZnO semiconductor from the Zn LMM, Zn2p, and O1s electron spectra. The valence band maximum (VBM) was roughly estimated by extrapolating the linear part of the spectra, and both ZnO layers prepared at −1.4 and −5.0 mAcm^{-2} showed almost constant value of 2.9 eV. The value of 2.9 eV corresponded to the energy difference between the valence band maximum (VBM) and Fermi level (E_F), since the 0 eV in the binding energy corresponded to the Fermi level in the sample. The value of 2.9 eV was consistent with that already reported for the ZnO semiconductor.[21] The energy difference between the conduction band minimum (CBM, E_c) and Fermi level (E_F) was estimated to be 0.35 and 0.42 eV for the ZnO layers prepared at −1.4 and −5.0 mAcm^{-2}, respectively, from the bandgap energy estimated from the absorption edge and

energy difference between valence band maximum (VBM) and Fermi level (E_F).

The relation between the energy difference (E_c-E_F) and carrier concentration(n) is *represented* as follows:
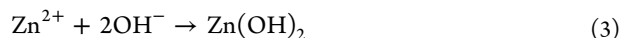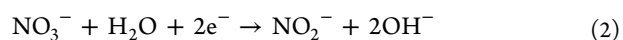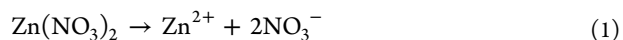
$$E_c - E_F = KT\ln(N_c/n)$$

where K, T, and N_c are the Boltzmann constant, temperature, and effective density of state in the conduction band.[22] This relation indicates that the energy difference (E_c-E_F) decreased with the increase in the carrier concentration corresponding to the donor density in an n-type semiconductor, until the donor density (n) equals the effective density of state (N_c). According to the relation, it was speculated that the energy difference (E_c-E_F) for the ZnO layer prepared at −1.4 mAcm^{-2} was lower than that at −5.0 mAcm^{-2} from the already mentioned carrier concentration, and the speculation was consistent with the experimental result.

The preferred orientation of ZnO layers changed from (0001) to random orientation and the resistivity increased with increase in cathodic current density. The tendency is consistent with those already reported in detail.[20] The (0001) plane apt to be parallel to the surface at the condition close to the equilibrium state, because of the lowest surface energy in the wurtzite ZnO crystal.[23] The increase in the deposition rate relating to the cathodic current density induced the growth of $(11\underline{2}0)$ and $(10\underline{1}0)$ planes, resulting in the formation of random orientation. The resistivity (ρ) of ZnO layers increased with increase in cathodic current density and can be calculated by following equation;

$$1/\rho = qn\mu$$

,where q, n, and μ represent the elemental charge, carrier concentration, and mobility. It is generally agreed for undoped ZnO semiconductor that the carrier was due to the excess zinc attributed to either an oxygen vacancy or interstitial zinc atoms, which act as a donor, and the carrier concentration is closely related to the oxygen-deficient nonstoichiometry. The mobility are mainly limited by scattering defects such as impurities and lattice defects including the grain boundary.

The authors reported that the dependence of the preferred orientation of electrodeposited Cu$_2$O and Ag$_2$O semiconductors on the cathodic current density could be reasonably explained by considering the formation rate of metal hydroxides, which were the precursor of Cu$_2$O and Ag$_2$O.[24] The deposition mechanism for the ZnO deposition is described as follows;[25]

$$Zn(NO_3)_2 \rightarrow Zn^{2+} + 2NO_3^- \qquad (1)$$

$$NO_3^- + H_2O + 2e^- \rightarrow NO_2^- + 2OH^- \qquad (2)$$

$$Zn^{2+} + 2OH^- \rightarrow Zn(OH)_2 \qquad (3)$$

$$Zn(OH)_2 \rightarrow ZnO + H_2O \qquad (4)$$

The elementally formation rate (ν) of Zn(OH)$_2$, which was the precursor of ZnO, on the substrate can be expressed as;

$$\nu = k[Zn^{2+}][OH^-]^2$$

,where k represents the rate constant. The concentration of hydroxide ion, [OH$^-$], increased with increase in cathodic current density corresponding to the amount of electrons, according to the reaction2. The concentration of zinc cation, [Zn^{2+}], was constant in the present experiment. The increase in

9389

dx.doi.org/10.1021/am403137x | ACS Appl. Mater. Interfaces 2013, 5, 9386−9395

cathodic current density induced the relative increase of $[OH^-]$ to $[Zn^{2+}]$ concentration, which would result in decrease in oxygen vacancy, which act as a donor in the resultant ZnO layer. Also, the increase in cathodic current density induced the increase in the elemental formation rate with the assumption of current efficiency of 100%, resulting in the change in the preferred orientation of the ZnO layers.

3.2. Optical, Structural, And Electrical Characteristics of Hybrid Phthalocyanine/n-ZnO Photovoltaic Devices with and without ZnO Buffer Layer. Figure 4 shows the
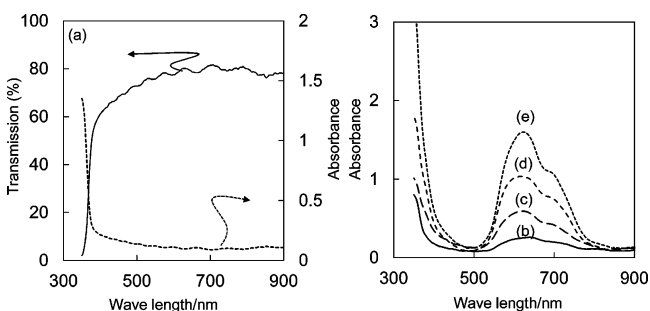
Figure 4. (a) Transmission and absorption spectra for ZnO buffer/n-ZnO layers and absorption spectra for (b) 50, (c) 100, (d) 200, and (e) 400 nm thick phthalocyanine/ZnO buffer/n-ZnO layers.

optical transmission spectra for the ZnO buffer/n-ZnO layers and absorption spectra for the 50−400-nm-thick-phthalocyanine/ZnO buffer/n-ZnO layers prepared on FTO substrate. The ZnO buffer/n-ZnO layer showed an optical transmission at approximately 80% at wavelengths ranging from 900 to 600 nm, and the transmission gradually decreased with the decreasing wavelength. The transmission rapidly decreased at around 380 nm in wavelength and absorbance rapidly increased, because of the electron excitation from the valence band to the conduction band in ZnO layers by absorbing light at a wavelength shorter than the absorption edge related to the band gap energy. The absorption spectra were the same in profile and absorption edge for the n-ZnO layers with and without the ZnO buffer layer, because of the thin thickness of the ZnO buffer layer.

The phthalocyanine/ZnO buffer/n-ZnO hybrid photovoltaic devices showed an absorption peak and shoulder at the wavelengths of 636 and 700 nm corresponding to the photon energy of 1.94 and 1.76 eV, respectively. The absorbance at 1.94 and 1.76 eV increased with an increase in the thickness of the phthalocyanine from 50 to 400 nm. Also, the absorbance at a wavelength of about 380 nm increased with an increase in the phthalocyanine thickness. The increase in absorbance originated from the phthalocyanine layer, since the ZnO layers with the absorption edge at around a 380 nm wavelength possessed a constant thickness.

The phthalocyanine powder dissolved in benzene showed two strong and two weak absorption bands at the wavelengths of 700, 660, 600, and 350 nm corresponding to the photon energy of 1.77, 1.88, 2.07, and 3.54 eV, respectively, and the profile and the peak photon energy changed depending on the solvent.[26] The phthalocyanine layer prepared on a quartz glass substrate by vacuum evaporation showed two peaks and a shoulder at the wavelengths of 346, 632, and 700 nm corresponding to the peak energy of 3.58, 1.96, and 1.77 eV, respectively. The peak energies were close to those observed for the hybrid phthalocyanine/ZnO buffer/n-ZnO photovoltaic

devices. The difference in the absorption spectra among the dissolved phthalocyanine powders and the thin layers suggested that the configuration of the phthalocyanine molecules affected the profile and absorbance in the absorption spectra. The absorption peaks at wavelengths ranging from 500 to 800 nm were assigned as the Q-band n →π* transition, and the absorption below 400 nm was identified as the π →π* transition of the Soret band.[27] The absorption coefficients calculated for the absorbance and thickness were 5.2×10^4, 5.9×10^4, 5.2×10^4, and 4.0×10^4 cm^{-1} for the thicknesses of 50, 100, 200, and 400 nm, respectively.

Figure 5 shows the X-ray diffraction patterns for the hybrid 50−400 nm thick phthalocyanine/ZnO buffer/n-ZnO photo-
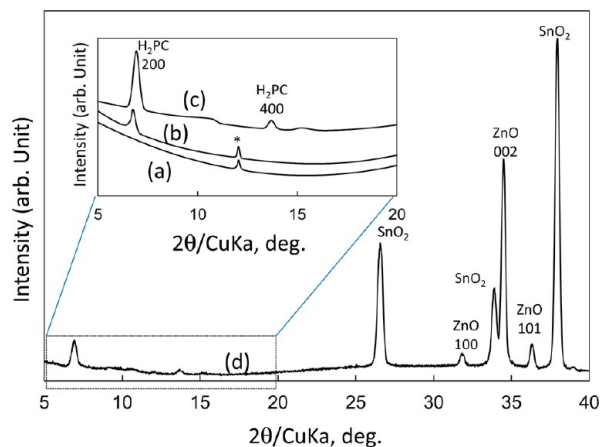
Figure 5. X-ray diffraction patterns for (a) 50, (b) 100, and (c, d) 200 nm thick phthalocyanine/ZnO buffer/n-ZnO photovoltaic devices.

voltaic devices. Some peaks were observed at 2θ angles ranging from 25 to 40° and could be identified as those for ZnO with the characteristic wurtzite lattice[28] and tetragonal SnO_2 of the substrate.[29] The X-ray diffraction patterns had the same profile and peak angles for the hybrid photovoltaic devices with and without the ZnO buffer layer. The lattice parameters for the ZnO layer were calculated from the peak angles referenced to those for the SnO_2 with the lattice parameter of 4.7382 Å in a-axis and 3.1871 Å in c-axis. The lattice parameters of 3.250 Å in a-axis and 5.207 Å in c-axis could be obtained for the ZnO layer, and the values nearly agreed with those tabulated on the ICDD card.[28] The (0002) diffracted X-ray peak was relatively strong compared to the (10$\underline{1}$0) and (10$\underline{1}$1) peaks, indicating that the ZnO layer possessed a slight (0002) preferred orientation.

The diffracted X-ray peaks that originated from the phthalocyanine layers could be observed at 2θ angles ranging from 5 to 15°, and the intensity was weak compared to those for the ZnO and SnO_2 layers. Two peaks could be observed at 6.86 and 13.56° for the 200 nm thick phthalocyanine-layer-deposited ZnO layer and were identified as the (200) and (400) peaks of α-phthalocyanine with the monoclinic lattice of 26.121 Å in a-axis, 3.797 Å in b-axis, 23.875 Å in c-axis, and a 94.16° in β-angle,[30] indicating that the 200 nm thick phthalocyanine layer possessed a (200) preferred orientation. The intensity of the (200) peak weakened and the (400) peak disappeared for the 100 nm thick phthalocyanine layer, whereas a peak appeared at 12.02°. The (200) peak disappeared for the 50 nm thick phthalocyanine layer, whereas only one peak with a weak intensity remained at 12.02°. The peak at 12.02° could
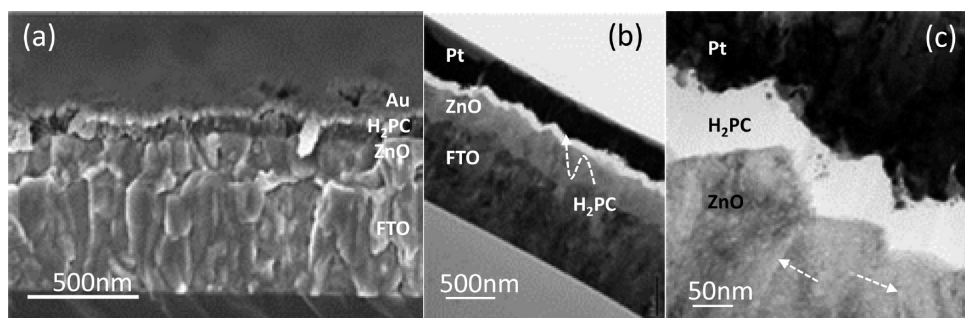
Figure 6. Cross-sectional structures of the layered 50 nm thick phthalocyanine/ZnO buffer/n-ZnO/FTO hybrid photovoltaic device with (a) FE-SEM and (b, c) FE-TEM.

not be assigned as any peaks related to the α-phthalocyanine, but the peak angle was close to that for the (002) plane of phthalocyanine with a monoclinic lattice of 17.31 Å in a-axis, 4.72 Å in b-axis, 14.8 Å in c-axis, and a 104 degree in β-angle, as tabulated on the ICDD card.[31]

Figure 6 shows the cross-sectioned structure of the hybrid 50-nm-thick-phthalocyanine/ZnO buffer/n-ZnO photovoltaic device with FE-SEM and FE-TEM. The ZnO layer possessed a thickness of approximately 300 nm and was composed of n-ZnO and ZnO buffer layers prepared by controlling the cathodic current density during the ZnO electrodeposition. The thickness of the ZnO buffer layer was calculated to be approximately 15 nm from the electric change. The interface between the n-ZnO and ZnO buffer layers, however, could not be observed in the FE-SEM image. The ZnO layer was composed of aggregates of columnar grains grown in a direction normal to the substrate surface, and the vertical size of the columnar ZnO grains corresponded to the layer thickness. The width of the columnar ZnO grains was estimated to be approximately 76 nm. Defects such as pores, could not be located both throughout the ZnO thickness and at the interface of the glass substrate. The 50 nm thick phthalocyanine layer homogenously stacked over entire the ZnO surface and was composed of aggregates of columnar grains grown in a direction normal to the substrate surface, and the width of the phthalocyanine grains was estimated to be approximately 48 nm. Granular grains with the size of approximately 20 nm could be partly observed at near the heterointerface to the ZnO layer, and the heterointerface between the ZnO and phthalocyanine layers could be clearly observed. The insertion of the ZnO buffer layer showed no effects on the morphology of the phthalocyanine layer as well as the X-ray diffraction patterns.

The ZnO and phthalocyanine layers, which showed a slightly dark and bright appearance, could be clearly observed between the FTO and Pt layers, and the heterointerface between the ZnO and phthalocyanine layers could be clearly observed on the FE-TEM image (Figure 6b). The ZnO layer was composed of large grains, and the grain boundaries represented by arrow could be observed inside the ZnO layer. The interface between the n-ZnO and ZnO buffer layers, however, could not be observed inside the ZnO grain even on the magnified image (Figure 6c). These facts suggested that the ZnO buffer layer heteroepitaxially grew up on the n-ZnO layer, because that the lattice constants were almost the same for both the ZnO layers.[23]

The thickness of the phthalocyanine layer increased with an increase in the deposition time, and the phthalocyanine layer possessed almost the same columnar structure, irrespective of the thickness, in spite of the fact that the lattice parameters and preferred orientation changed. It was reported that the preferred orientation of the phthalocyanine layer strongly depended on the substrate material and orientation in the weak epitaxial growth.[32] It was confirmed that (200)-oriented α-phthalocyanine layers at the thickness ranging from 50 to 400 nm were formed on a quartz glass substrate without any lattice relationship to the phthalocyanine crystal, indicating that the (200) plane apt to be parallel to the substrate surface at the condition used in this study. The change in the X-ray diffraction profile suggested that the structure of under ZnO layer affected the structure and orientation of the 50 nm thick phthalocyanine layer deposited at the initial stage, and the structure and orientation changed during the growth, keeping the characteristic optical absorption feature.

The 400 nm thick phthalocyanine layer prepared on a quartz glass substrate showed a resistivity on the order of 1×10^8 Ω cm, whereas the resistivity could not be estimated for the 50–200 nm thick phthalocyanine layers because of the high resistivity. The resistivity was close to those already reported for the phthalocyanine crystal[33] and copper phthalocyanine.[34]
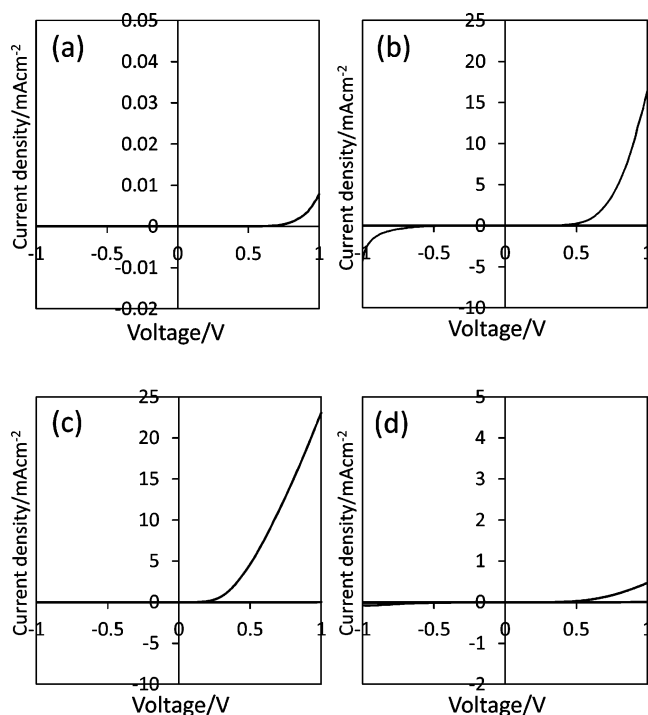
Figure 7 shows the current density–voltage curves for the hybrid phthalocyanine/n-ZnO and phthalocyanine/ZnO buffer/n-ZnO photovoltaic devices in dark. The rectification ratio was estimated by calculating the ratio of the current densities at voltages of ±1.0 V. It is generally accepted for inorganic p-n heterojunction diodes that the relation between the forward current density (J_F) and forward voltage (V_F) is represented by the following empirical formula

$$J_F \propto \exp(qV_F / \eta KT)$$

where K, q, T, and η are the Boltzmann constant, elemental change, temperature, and ideality factor, respectively.[35] This relation is used for characterizing the p–n junction diodes composed of inorganic semiconductors, and the ideality factor equals 1 when the diffusion current dominates and equals 2 when the recombination current dominates. All the hybrid phthalocyanine/ZnO photovoltaic devices showed a rectification feature in dark, irrespective of the insertion of the ZnO buffer layer.

The ZnO buffer-free hybrid 50 nm thick phthalocyanine/n-ZnO photovoltaic device showed a rectification feature of 3300 in rectification ratio, but the forward current density was limited at the very low level of 7.86 μA cm^{-2}. The ideality factor was estimated to be 7.33.

The insertion of the ZnO buffer layer between the n-ZnO and 50 nm thick phthalocyanine layers induced a drastic increase in the forward current density to 16.5 mA cm^{-2}, which
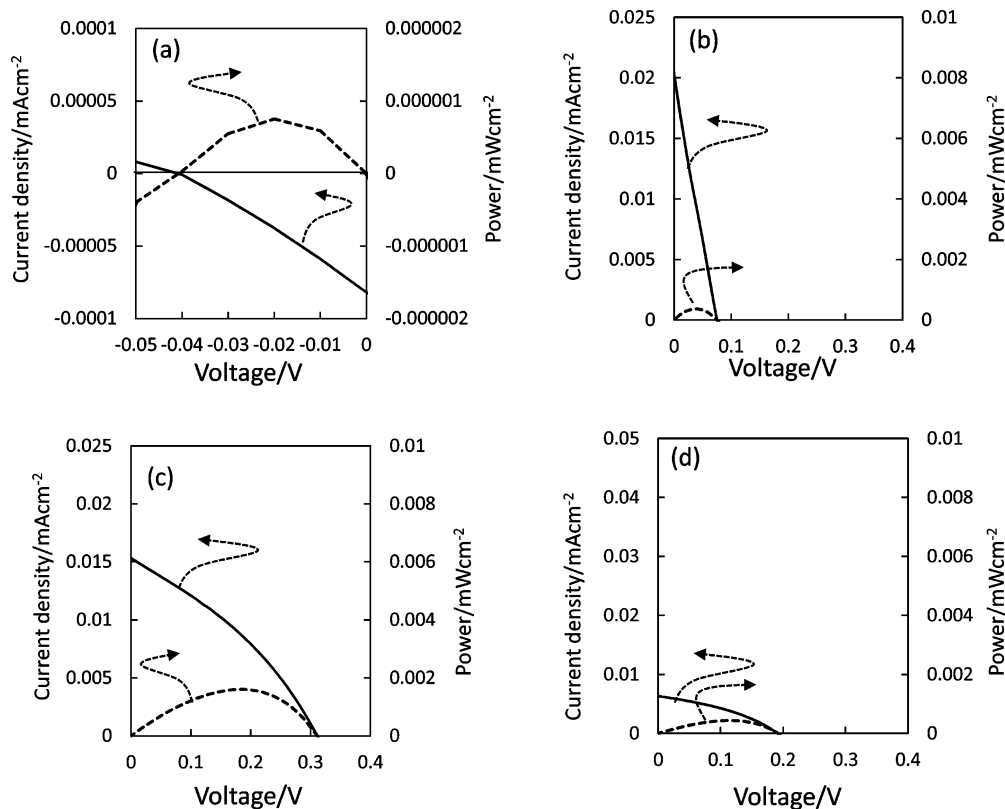
Figure 7. Current density—voltage curves recorded for (a) 50 nm thick phthalocyanine/n-ZnO and hybrid (b) 50, (c) 200, and (d) 400 nm thick-phthalocyanine/ZnO buffer/n-ZnO photovoltaic devices in dark.

was about two thousand times that for the ZnO buffer free hybrid phthalocyanine/n-ZnO photovoltaic device, and the

ideality factor of approximately 1.0, which corresponded to that when the diffusion current dominates in inorganic p-n heterojunction diodes, was obtained. The rectification ratio, however, deteriorated from 3300 to 3.8 by inserting the ZnO buffer layer, because of the increase in the leakage current density. The increase in the thickness of the phthalocyanine layer from 50 to 200 nm induced an increase in the forward current density to 23.1 mA cm^{-2} and improvement of the rectification ratio from 3.8 to 3188 due to the suppression of the leakage current density. The ideality factor was estimated to be 1.29 between 1 for the diffusion current domination and 2 for recombination current domination. The increase in the phthalocyanine thickness to 400 nm induced the suppression of the forward current density to 0.473 mAcm^{-2} and reduction of the rectification ratio to 692. The ideality factor increased to 7.3. The deterioration of the rectification feature with an increase in the phthalocyanine thickness from 200 to 400 nm was attributed to the high resistivity of the phthalocyanine layer.

Figure 8 shows current density—voltage curves for the ZnO buffer-free and -inserted phthalocyanine/n-ZnO photovoltaic devices under AM1.5G illumination. The ZnO buffer-free hybrid phthalocyanine/n-ZnO photovoltaic device generated a negative photocurrent density at 0 V by irradiating AM1.5G-illumination. It was predicted that a positive photocurrent would be generated by the AM1.5G illumination from the energy diagram. The short circuit current density (J_{SC}) and open-circuit voltage (V_{OC}) are estimated to be -8×10^{-5} mA cm^{-2} and -0.041 V, respectively, and the conversion efficiency was calculated to be 7.5×10^{-7} % for the ZnO-buffer-free-hybrid 50-nm-thick phthalocyanine/n-ZnO photovoltaic de-

Figure 8. Current density—voltage and power—voltage curves recorded for (a) 50 nm thick-phthalocyanine/n-ZnO and hybrid (b) 50, (c) 200, and (d) 400 nm thick phthalocyanine/ZnO buffer/n-ZnO photovoltaic devices under AM1.5G-illumination.

vice. It was confirmed that the current density was very close to 0 mA cm^{-2} at 0 V in dark on the same vertical scale. The conversion efficiency was consistent with those already reported for the phthalocyanine/ZnO photovoltaic devices.[4]

The insertion of the ZnO buffer layer between the n-ZnO and 50-nm-thick phthalocyanine layers induced the change to the positive side and the increase in the short circuit current density to 0.02 mAcm^{-2}, which was about 250 times that for the ZnO buffer-free-hybrid 50-nm-thick phthalocyanine/n-ZnO photovoltaic device. The open-circuit voltage (V_{OC}) increased to 0.08 V by the ZnO buffer insertion, resulting in the increased conversion efficiency to 3.6×10^{-4} %, which was about 500 times that for the ZnO-buffer-free-hybrid 50-nm-thick phthalocyanine/n-ZnO photovoltaic device. The increase in the phthalocyanine thickness from 50 to 200 nm along with the constant thickness of the ZnO buffer layer gave the increase in the open-circuit voltage (V_{OC}) to 0.31 V, although the short circuit current density (J_{SC}) slightly decreased to 0.015 mAcm^{-2}. The conversion efficiency was calculated to be about 0.0016%, which was about 2,100 times that for the ZnO-buffer-free-hybrid 50-nm-thick phthalocyanine/n-ZnO photovoltaic device. The increase in the phthalocyanine thickness to 400 nm induced a decrease in both the open-current voltage (V_{OC}) to 0.19 V and short circuit current density (J_{SC}) to 6×10^{-3} mAcm^{-2}, and the conversion efficiency decreased to 4.3×10^{-3} %.

The insertion of the ZnO buffer layer between the n-ZnO and phthalocyanine layers induced drastic improvements in both the rectification feature in dark and photovoltaic performance under AM1.5G illumination, and a most excellent rectification feature and photovoltaic performance could be obtained for the hybrid 200-nm-thick phthalocyanine/ZnO buffer/n-ZnO photovoltaic device. It is accepted for organic photovoltaic devices that the short circuit current density is closely related to the diffusion length of the excitons generated in organic semiconductors by light irradiation.[36] The exciton diffusion length was reported to be 10 ± 3 nm for the Cu-phthalocyanine layer prepared by high vacuum evaporation of the purified raw materials.[36] The diffusion length of 11.9 nm was reported for the metal-free phthalocyanine prepared by thermal evaporation.[37] The thickness of the phthalocyanine layer used in this study would be greater than the diffusion length of the excitons generated in the phthalocyanine layer, but the thickness was not sufficient to absorb the light because of the calculated absorption coefficient. Since the grain structure and absorption feature of the phthalocyanine layers were not affected by the insertion of the ZnO buffer layer, the diffusion length of the excitons would be constant for both phthalocyanine/ZnO photovoltaic devices.

Mcghee and co-workers extensively investigated the characteristics of hybrid photovoltaic devices composed of inorganic semiconductors of TiO$_2$ and CdSe and organic polymer semiconductors of P3HT, MEH-PPV, and OC$_1$C$_{10}$-PPV and the effects of the surface modification of the inorganic semiconductors.[7] The importance of the molecular dipole and acid−base interaction was pointed out causing the band-edge shift in the inorganic semiconductor followed by the change in the V_{OC}. It was generally accepted for inorganic photovoltaic device, such as the Cu(InGa)Se$_2$ solar cell, that the band alignment at the heterointerface was important for transport of the carriers generated in the light-absorbing layer.[38] The bandgap energy was 3.25 and 3.32 eV for the n-ZnO and ZnO buffer layers, respectively, and the energy difference between

the valence band maximum (VBM) and Fermi level (E_F) was constant at 2.9 eV. The work function was reported to be 4.5 eV for the ZnO semiconductor,[39] and the work function was assumed to be constant for both ZnO layers. The LUMO and HOMO level were reported to be 3.9 and 5.2 eV for the metal-free phthalocyanine under vacuum level.[40] The band alignment near the heterointerface between the n-ZnO and phthalocyanine layers could be considered based on the energy states of the n-ZnO, ZnO buffer, and phthalocyanine. The built-in-potential was formed at the heterointerface between the n-ZnO and phthalocyanine layers. The insertion of the ZnO buffer layer between the n-ZnO and phthalocyanine layers induced the formation of the spike-type conduction band offset of approximately 0.07 eV at the heterointerface, and the interfacial layer including the depletion layer widened by the ZnO buffer layer insertion. It is generally accepted that the insertion of buffer layers with an optimum bandgap energy and ionization energy effectively enhanced the photovoltaic performance of inorganic photovoltaic devices of Cu(InGa)Se$_2$. The photovoltaic performance is closely related to the conduction band offset formed by the inserted buffer layer at the heterointerface, and a spike-type conduction band offset of 0.1 to 0.3 eV is favorable to suppress the recombination of carriers at the heterointerface.[38] The ZnO buffer-free hybrid phthalocyanine/n-ZnO photovoltaic devices showed a poor performance with a 0.04 V open-current voltage and 8×10^{-5} mAcm^{-2} short circuit current density. The ZnO layers prepared by electrodeposition contained some amount of impurities and native defects, such as interstitial zinc atoms and vacancies.[41] The poor photovoltaic performance suggested that the native defects located in the n-ZnO layer near the heterointerface to the phthalocyanine layer act as sites for the recombination of carriers generated in the phthalocyanine layer. The inserted ZnO buffer layer could form the spike-type conduction band offset of 0.07 eV, and the recombination of carriers was suppressed by this conduction band offset.

The trap level at energy within the forbidden gap and within the space charge region is accepted to act as the recombination site in inorganic photovoltaic devices such as Cu(InGa)Se$_2$/CdS/ZnO solar cell.[42,43] The existence of the conduction band offset affected the amounts of electron and holes injected toward the heterointerface, resulting in the change in recombination rate via trap level, commonly referred to as Schockley-Read-Hall recombination.[44] Also, the presence of the trap-induced recombination were reported for the P3HT:PCBM organic solar cell.[45] The band alignment including the conduction band offset is an important factor affecting the photovoltaic performance of the hybrid photovoltaic devices, although further investigation and theoretical consideration are needed.

The insertion of ZnO buffer layer between the n-ZnO and phthalocyanine layers induced the improvement of the photovoltaic performance, but the active layer to generate the carrier from sunlight is still limited to the region near the heterointerface because of the small diffusion length of carrier and excitons. The introduction of nanostructures like the buk-heterojunction structure of organic photovoltaic devices should be considered to improve the photovoltaic performance because of the increase in the active region within organic absorbing layer.

9393

dx.doi.org/10.1021/am403137x | ACS Appl. Mater. Interfaces 2013, 5, 9386−9395

4. CONCLUSIONS

A layered hybrid photovoltaic device composed of metal-free-phthalocyanine and ZnO layers were constructed by electrodeposition of the ZnO layer followed by vacuum evaporation of the phthalocyanine layer. ZnO layers with the resistivity of 1.6×10^3 and 1×10^8 Ω were prepared by controlling the cathodic current density in a simple zinc nitrate hydrate aqueous solution and were installed in the hybrid photovoltaic devices as n-ZnO and ZnO buffer layers, respectively. The phthalocyanine layer possessed a characteristic absorption feature irrespective of the thickness from 50 to 400 nm, although the lattice parameter and preferred orientation changed depending on the thickness. The ZnO buffer-free hybrid 50-nm-thick-phthalocyanine/n-ZnO photovoltaic device showed a rectification feature in dark, but the photovoltaic performance was very poor with a 0.041 V in open circuit voltage, 8×10^{-5} mA cm^{-2} in short circuit current density, and conversion efficiency of 7.5×10^{-7} %.

The insertion of the ZnO buffer layer between the n-ZnO and 50-nm-thick phthalocyanine layers induced improvements in both rectification features in dark and photovoltaic performance. The insertion of the ZnO buffer layer induced an increase in the forward current density at 1.0 V from 7.86×10^{-3} to 16.48 mAcm^{-2} and improvement of the ideality factor from 7.33 to 1.04. The 50 nm thick phthalocyanine/ZnO buffer/n-ZnO photovoltaic device showed an improved photovoltaic performance of a 0.08 V in open circuit voltage, 0.02 mA cm^{-2} short circuit current density, and conversion efficiency of 3.6×10^{-4} %, which was approximately 500 times that for the ZnO buffer-free phthalocyanine/n-ZnO photovoltaic device. The best performance was obtained for the 200 nm thick phthalocyanine/ZnO buffer/n-ZnO photovoltaic device with an excellent rectification feature of the rectification ratio of 3188, forward current density of 23.1 mA cm^{-2}, and ideality factor of 1.29. The open circuit voltage of 0.31 V, short circuit current density of 0.015 mA cm^{-2}, and conversion efficiency of 1.6×10^{-3} % were obtained for the hybrid 200-nm-thick-phthalocyanine/ZnO buffer/n-ZnO photovoltaic device, and the conversion efficiency was about 2100 times that for the ZnO buffer-free hybrid phthalocyanine/n-ZnO photovoltaic device. The improvement in both the rectification feature and photovoltaic performance by the ZnO buffer insertion was attributed to the formation of the spike-type conduction band offset at the heteroinerface between the n-ZnO and phthalocyanine layers, resulting in suppression of the recombination loss. The results demonstrated here indicated the importance of the band alignment even in a hybrid photovoltaic device as pointed out for the inorganic photovoltaic devices such as Cu(InGa)Se$_2$ solar cells.

ASSOCIATED CONTENT

ⓢ Supporting Information

The resistivity, carrier concentration, and mobility for ZnO layers preparaed at cathodic current density ranging from 0.1 to 5 mA cm^{-2}. This material is available free of charge via the Internet at http://pubs.acs.org/.

AUTHOR INFORMATION

Corresponding Author

*E-mail: m-izaki@me.tut.ac.jp.

Notes

The authors declare no competing financial interest.

REFERENCES

(1) McGehee, M. D. *MRS Bull.* **2009**, *34*, 95−100.
(2) Beek, W. J. E.; Wienk, M. M.; Kemerink, M.; Yang, X.; Janssen, R. A. J. *J. Phys. Chem.B* **2005**, *109*, 9505−9516.
(3) Coakley, K. M.; McGehee, M. D. *Appl. Phys. Lett.* **2003**, *83*, 3380−3382.
(4) Stakhira, P. I.; Pakhomov, G. L.; Cherpak, V. V.; Volynyuk, D.; Luka, G.; Godlewski, M.; Guziewicz, E.; Hotra, Z. Y. *Cent. Eur. J. Phys.* **2010**, *8*, 798−803.
(5) Coakley, K. M.; McGehee, M. D. *Chem. Mater.* **2004**, *16*, 4533−4542.
(6) Beek, W. J. E.; Wienk, M. M.; Janssen, R. A. J. *Adv. Mater.* **2004**, *16*, 1009−1013.
(7) Vaynzof, Y.; Kabra, D.; Zhao, L.; Ho, P. K. H.; Wee, A. T. S.; Friend, R. H. *Appl. Phys. Lett.* **2010**, *97*, 033309−033309−3.
(8) Goh, C.; Scully, S. R.; McGehee, M. D. *J. Appl. Phys.* **2007**, *101*, 114503−114503−12.
(9) Yoshida, Y.; Nakamura, M.; Tanaka, S.; Hiromitsu, I.; Fujita, Y.; Yoshino, K. *Synth. Met.* **2006**, *156*, 1213−1217.
(10) Hiramoto, M.; Fujiwara, H.; Yokoyama, M. *Appl. Phys. Lett.* **1991**, *58*, 1062−1064.
(11) Tang, C. *Appl. Phys. Lett.* **1986**, *48*, 183−185.
(12) Izaki, M.; Saito, T.; Ohata, T.; Murata, K.; Fariza, B. M.; Sasano, J.; Shinagawa, T.; Watase, S. *ACS Appl. Mater. Interfaces* **2012**, *4*, 3558−3565.
(13) Izaki, M.; Shinagawa, T.; Mizuno, K.; Ida, Y.; Inaba, M.; Tasaka, A. *J. Phys. D: Appl. Phys.* **2007**, *40*, 3326−3329.
(14) Sakai, K.; Hiramoto, M. *Mol. Cryst. Liq. Cryst.* **2008**, *491*, 284−289.
(15) Terada, N.; Widodo, R.; Itoh, K.; Kong, S.; Kashiwabara, H.; Okuda, T.; Obara, K.; Niki, S.; Sakurai, K.; Yamada, A. *Thin Solid Films* **2005**, *480*, 183−187.
(16) Izaki, M.; Omi, T. *Appl. Phys. Lett.* **1996**, *68*, 2439−2440.
(17) Izaki, M.; Omi, T. *J. Electrochem. Soc.* **1997**, *144*, L3−L5.
(18) Ahmed, S.; Reuter, K. B.; Gunawan, O.; Guo, L.; Romankiw, L. T.; Deligianni, H. *Adv. Energy. Mater.* **2012**, *2*, 253−259.
(19) Lincot, D.; Guillemoles, J. F.; Taunier, S.; Guimard, D.; Sicx-Kurdi, J.; Chaumont, A.; Roussel, O.; Ramdani, O.; Hubert, C.; Fauvarque, J. *Sol. Energy* **2004**, *77*, 725−737.
(20) Shinagawa, T.; Chigane, M.; Murase, K.; Izaki, M. *J. Phys. Chem. C* **2012**, *116*, 15925−15931.
(21) Zhu, Y.; Chen, G.; Ye, H.; Walsh, A.; Moon, C.; Wei, S. H. *Phys. Rev. B* **2008**, *77*, 245209−245209−7.
(22) Sze, S. M.; Ng, K. K. *Physics of Semiconductor Devices*, 3rd ed.; Wiley−Interscience: Hoboken, NJ, 2007, p 99.
(23) Izaki, M.; Omi, T. *J. Electrochem. Soc.* **1997**, *144*, 1949−1952.
(24) Shinagawa, T.; Ida, Y.; Mizumo, K.; Watase, S.; Watanabe, M.; Inaba, M.; Tasaka, A.; Izaki, M. *Cryst. Growth Des.* **2013**, *13*, 52−58.
(25) Izaki, M.; Omi, T. *J. Electrochem. Soc.* **1996**, *143*, L53−L55.
(26) Fielding, P.; Gutman, F. *J. Chem. Phys.* **1957**, *26*, 411−419.
(27) Seoudi, R.; El-Bahy, G.; El Sayed, Z. *Opt. Mater.* **2006**, *29*, 304−312.
(28) *Powder Diffraction File 41-1445*; Joint Comittee on Powder Diffraction Standards, International Centre for Diffraction Data: Swarthmore, PA, 1992.
(29) *Powder Diffraction File 36-1451*; Joint Comittee on Powder Diffraction Standards, International Centre for Diffraction Data: Swarthmore, PA, 1992.
(30) Janczak, J. *Pol. J. Chem.* **2000**, *74*, 157−162.
(31) *Powder Diffraction File 2-312*; Joint Comittee on Powder Diffraction Standards, International Centre for Diffraction Data: Swarthmore, PA, 1992.
(32) Qiao, X.; Huang, L.; Zhang, J.; Tian, H.; Geng, Y.; Yan, D. *J. Phys. Chem. B* **2012**, *116*, 1812−1818.

9394

dx.doi.org/10.1021/am403137x | *ACS Appl. Mater. Interfaces* 2013, 5, 9386−9395

(33) Pakhomov, G. L. *Solid State Commun.* **2005**, *134*, 491−495.

(34) Hassan, A.; Ray, A.; Gould, R. *Phys. Status Solidi (a)* **1996**, *158*, K23−K25.

(35) Sze, S. M.; Ng, K. K.; *Physics of Semiconductor Devices*, 3rd ed.; Wiley−Interscience: Hoboken, NJ, 2007; p 99.

(36) Peumans, P.; Yakimov, A.; Forrest, S. R. *J. Appl. Phys.* **2003**, *93*, 3693−3723.

(37) Terao, Y.; Sasabe, H.; Adachi, C. *Appl. Phys. Lett.* **2007**, *90*, 103515−103515−3.

(38) Minemoto, T.; Hashimoto, Y.; Satoh, H.; Negami, T.; Takakura, H. *J. Appl. Phys.* **2001**, *89*, 8327−8330.

(39) Minami, T. *MRS Bull.* **2000**, 38−44.

(40) Hiramoto, M.; Fujiwara, H.; Yokoyama, M. *J. Appl. Phys.* **1992**, *72*, 3781−3787.

(41) Izaki, M.; Watase, S.; Takahashi, H. *Adv. Mater.* **2003**, *15*, 2000−2002.

(42) Rau, U.; Jasenek, A.; Schock, H. W.; Engelhardt, F.; Meyer, Th. *Thin Solid Films* **2000**, *361−362*, 298−302.

(43) Jasenek, A.; Schock, H. W.; Wermer, J. H.; Rau, U. *Appl. Phys. Lett.* **2001**, *79*, 2922−2924.

(44) Niemegeers, A.; Burgelman, M.; Herberholz, R.; Rau, U.; Haiskos, D. *Prog. Photovolt. Res. Appl.* **1998**, *6*, 407−421.

(45) Tzabari, L.; Tessler, N. *J. Appl. Phys.* **2011**, *109*, 064501−064501−5. <!——>